A low cost, disposable cable-shaped Al–air battery for portable biosensors

2016 J. Micromech. Microeng. 26 055011

(http://iopscience.iop.org/0960-1317/26/5/055011)

IOP Publishing Journal of Micromechanics and Microengineering
J. Micromech. Microeng. **26** (2016) 055011 (8pp) doi:10.1088/0960-1317/26/5/055011

A low cost, disposable cable-shaped Al–air battery for portable biosensors

Gareth Fotouhi[1], Caleb Ogier[2], Jong-Hoon Kim[3], Sooyeun Kim[4], Guozhong Cao[5], Amy Q Shen[6], John Kramlich[1] and Jae-Hyun Chung[1]

[1] Department of Mechanical Engineering, University of Washington, Seattle, WA 98195, USA
[2] Molecular Engineering and Sciences Institute, University of Washington, Seattle, WA 98195, USA
[3] School of Engineering and Computer Science, Washington State University, Vancouver, WA 98686, USA
[4] Mechanical Engineering, Korea Advanced Institute of Science and Technology (KAIST), Daejeon, Korea
[5] Materials Science and Engineering, University of Washington, Seattle, WA 98195, USA
[6] Micro/Bio/Nanofluidics Unit, Okinawa Institute of Science and Technology Graduate University, Okinawa, 904-0495, Japan

E-mail: jae71@uw.edu

Received 5 October 2015, revised 8 March 2016
Accepted for publication 29 March 2016
Published 19 April 2016

Abstract

A disposable cable-shaped flexible battery is presented using a simple, low cost manufacturing process. The working principle of an aluminum–air galvanic cell is used for the cable-shaped battery to power portable and point-of-care medical devices. The battery is catalyzed with a carbon nanotube (CNT)-paper matrix. A scalable manufacturing process using a lathe is developed to wrap a paper layer and a CNT-paper matrix on an aluminum wire. The matrix is then wrapped with a silver-plated copper wire to form the battery cell. The battery is activated through absorption of electrolytes including phosphate-buffered saline, NaOH, urine, saliva, and blood into the CNT-paper matrix. The maximum electric power using a 10 mm-long battery cell is over 1.5 mW. As a demonstration, an LED is powered using two groups of four batteries in parallel connected in series. Considering the material composition and the cable-shaped configuration, the battery is fully disposable, flexible, and potentially compatible with portable biosensors through activation by either reagents or biological fluids.

Keywords: battery, carbon nanotube, aluminum–air battery

S Online supplementary data available from stacks.iop.org/JMM/26/055011/mmedia

(Some figures may appear in colour only in the online journal)

1. Introduction

Point-of-care (POC) diagnostic systems are a rapidly growing field of portable devices [1]. POC diagnostic systems have evolved into a rapid and portable format, and are often disposed after a single usage [2–4]. Disposal POC devices require low-cost components including power sources to keep the assay cost low. Furthermore, devices for biomedical applications require power sources with stringent functionality including safety, stability, long shelf life, and high energy density [5]. When medical care is provided in remote areas or during disaster relief scenarios, conventional services of waste disposal are often unavailable. POC devices will therefore need to be equipped with light-weight and disposable batteries that will not pollute the local soil and aquatic environment when they are discarded.

Biological fluids and POC reagents have the potential to be used as electrolytes for power sources in disposable POC applications. POC reagents such as buffer solutions [6, 7] and alkaline solutions [8] could be used as electrolytes for power source operation. Most research uses physiological buffers and artificial bodily fluids [5–7, 9–13]. The use of real biological samples as the electrolyte for power sources is limited. Blood and sweat have been used as the electrolyte for a carbon

nanotube (CNT)/cellulose supercapacitor [14]. Small volumes of blood, urine, and saliva have been applied as the electrolyte for an aluminum–silver oxide battery [8]. Urine and saliva have also been used with magnesium–copper batteries [15, 16]. However, these biological fluid-activated batteries use a film shape that requires cumbersome manufacturing processes and costly materials that are inhibitive to low-cost, POC devices. In addition, placing toxic or contagious liquids on a battery may not be safe for operators and environment.

This work presents a cable-shaped aluminum–air (Al–air) battery for on-demand activation by biological fluids. A simple lathe-based manufacturing process is demonstrated for continuous battery fabrication, eliminating the need for cumbersome processing steps found in the biological fluid activated batteries and other cable-shaped batteries [17–19]. In this process, an Al wire is wrapped by a nanomaterial paper matrix composed of CNTs bound with cellulose fibers. The Al wire with the nanomaterial paper matrix is further wrapped with a silver-plated copper wire as a current collector. For a low-cost battery, all the material components are composed of mass-produced inexpensive materials and integrated by a series of lathe-based wrapping. This layered cable-shaped design allows for on-demand activation by absorbing biological fluids, which has yet to be demonstrated in a cable-shaped format. The battery performance is characterized by using electrolytes including potential reagents and biological- and physiological fluid samples. The cable-shaped battery is easily bent and cut for shape adaptive use and can be integrated into circuitry to obtain desired voltage and current.

2. Cable-shaped Al–air battery

A cable-shaped Al–O_2 battery integrated with a CNT-paper matrix is investigated (figure 1). An aluminum wire anode is wrapped with a CNT-paper matrix. The paper is then wrapped with a silver-plated copper wire to form the battery cell. The Al–O_2 electrochemical reaction is chosen because of its superior theoretical capacity over other battery systems [20]. Furthermore, aluminum is abundant, inexpensive, light-weight, and environmentally friendly. Since the cathode is oxygen, the weight and volume of the battery can be significantly reduced with a plentiful supply of oxygen from air. Figure 1 shows the major electrochemical reaction with the following reaction equations [20]:

$$\text{Aluminum anode}: 4Al(s) + 12OH^{-}(aq) \rightarrow 4Al(OH)_3(s) + 12e^{-} \quad (1)$$

$$\text{Cathode}: 3O_2(g) + 6H_2O(l) + 12e^{-} \rightarrow 12OH^{-}(aq) \quad (2)$$

$$\text{Overall reaction}: 4Al(s) + 3O_2(g) + 6H_2O(l) \rightarrow 4Al(OH)_3(s) \quad (3)$$

Since Al–O_2 systems do not carry the cathode species (O_2) within the cell, the catalytic efficiency at the cathode electrode strongly affects the anode reaction rate. An air-porous and electrically conductive layer should be used to allow O_2 to reach the catalyst layer. As a catalyst layer, CNTs embedded in paper enable efficient reduction of O_2 to hydroxide ions that are transported to the Al surface. A separating paper layer is wrapped between the catalyst and the Al anode. The porous paper layers also provide diffusion channels to draw the reaction product from the Al anode.

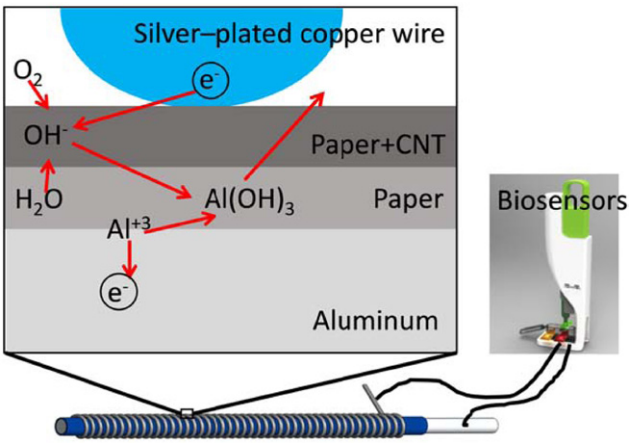

Figure 1. Configuration of a cable-shaped Al–oxygen battery. Al wire is wrapped with paper, CNT-paper matrix, and silver-plated copper wire sequentially. The battery is activated by depositing electrolytes into the paper layers.

3. Experimental method

The cable-shaped battery consisted of a core anode wire that was wrapped with two layers of low-density paper. The inner layer acted as a separation layer while the outer layer containing CNTs performed as a catalyst [20]. Both layers absorbed liquid-phase electrolyte and provided channels for transporting ions to the aluminum core. The paper layers were wrapped with a coil of silver-plated copper wire, which was electrically conductive to transport and distribute electrons to the CNTs. We chose this battery format to simplify the manufacturing process, to minimize the internal resistance, to minimize the distance between anode and cathode, and to maximize the surface area for oxygen reduction with a flexible format.

For scalable production using a lathe, a spool of 1.2 mm-diameter aluminum wire was purchased (The Hillman Group). Porous paper (KimWipes®) was cut into 400 mm long strips of 10 mm width and 0.06 mm thickness. The diameter of the silver-plated copper wire (Artistic Wire, PA, USA) was 0.16 mm. A CNT-paper layer was a key component that consisted of multi-walled carbon nanotubes (MWCNT) embedded into the cellulose matrix of porous paper (KimWipes®). A 5 mg ml^{-1} solution of MWCNTs (NanoAmor) was used to functionalize the surface of a paper matrix. The MWCNTs (outside diameter: 8–15 nm) were dispersed in 0.1% SDS (Fluka) through sonication (Bransonic Utlrasonic Cleaners Model 1510 − 40 kHz) for 2 h. Using a pipette, the MWCNT solution was serially deposited on the paper matrix to a density of 3 mg cm^{-2}. After each deposition, the paper was heated at 120 °C for 2 min to dry. Using a multimeter (Fluke 287/FVF), the measured resistance of a 10 mm-wide strip was 50–60 Ω/□.

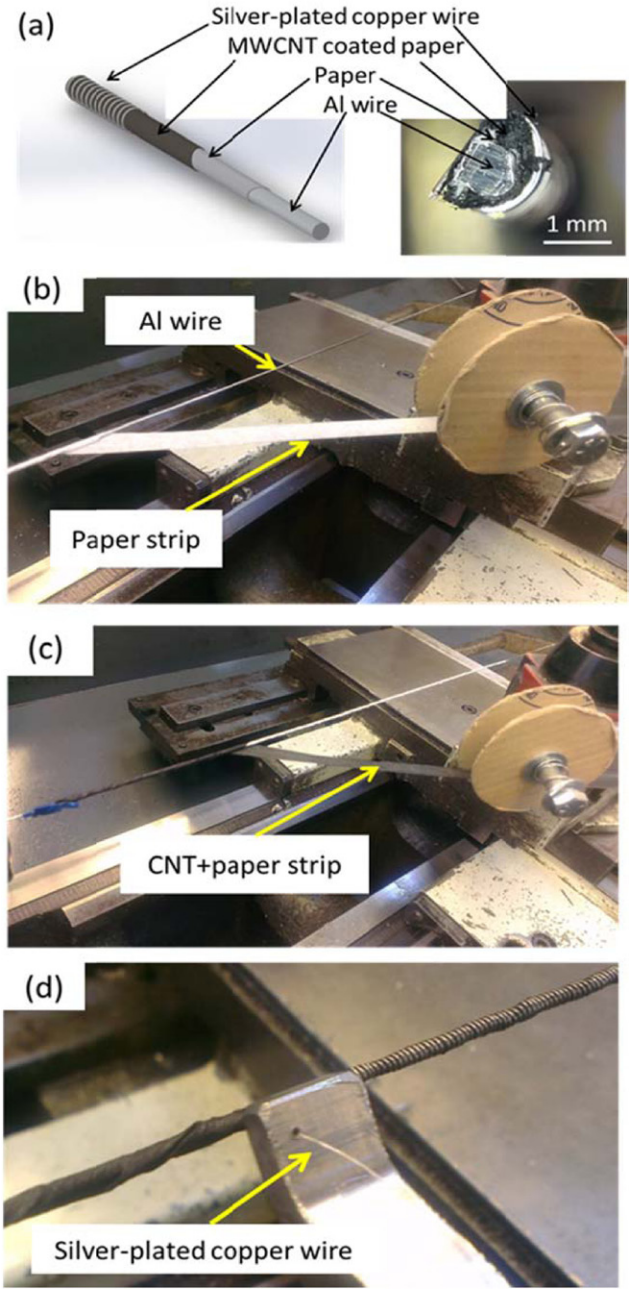

Figure 2. Structure and manufacturing process of a cable-shaped battery. (a) Configuration of a cable-shaped battery; Al wire wrapped with porous paper, CNT-paper and silver-plated copper wire, sequentially. The right photo shows the cross-section of a cable-shaped battery. (b) Wrapping of a porous paper strip. (c) Wrapping of a CNT-paper strip. (d) Wrapping of silver-plated copper wire.

For fabrication of a cable-shaped battery, the manufacturing process was automated using feeding spools for the porous paper, CNT-paper and silver-plated copper wire, respectively (figure 2(a)). The aluminum wire was suspended across a common machining lathe, allowing the aluminum wire to be rotated. As illustrated in figure 2(b), the aluminum wire was first wrapped in a paper strip. The CNT-paper was then wrapped over the non-coated paper (figure 2(c)). The silver-plated copper wire was the last material wrapped around the battery with a pitch of 0.75 mm (figure 2(d)). The

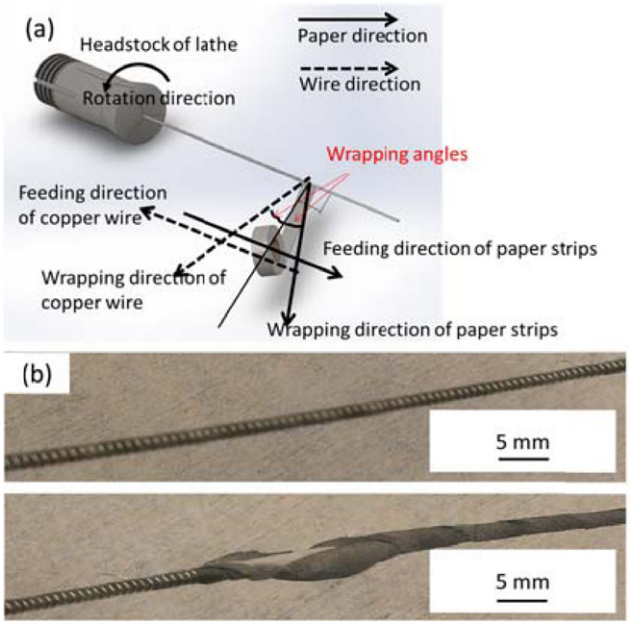

Figure 3. Rotational- and feeding directions for lathe-based manufacturing process. (a) Configuration of the rotation direction of a head stock and the feeding- and wrapping directions of the paper layers and the wire. (b) Cable-shaped batteries that are wrapped in uniform (top)- and nonuniform (bottom) ways.

cross-section of a fabricated battery is shown in figure 2(a) (image on the right).

When the wrapping was attempted on the lathe, the feeding- and wrapping directions for both paper strips and copper wire were found to be critical. When the headstock of the lathe rotated, the Al wire was continuously wrapped by the two paper layers as indicated by the solid arrows in figure 3(a). In the wrapping process, the wrapping angle should be close to 45° relative to the feeding direction such that the stress profile parallel to both edges of a paper strip should be uniform. An inappropriate feeding direction caused the paper strip to be conically wrapped on the aluminum wire, resulting in nonuniform wrapping of the paper strips.

When a silver-plated wire was wound on the paper-wrapped Al wire, the feeding- and wrapping directions were carefully chosen to maintain stable contact between the wrapped paper and the wire. When the feeding- and wrapping directions of the paper and the silver-plated copper wire were the same, the wrapped paper could be wiggled and peeled from the aluminum wire (figure 3(b)). As the winding of the silver-plated wire continued, the stress on the paper accumulated, resulting in nonuniform wrapping of the paper strip. Uniform winding was obtained when the feeding- and wrapping directions of the silver-plated copper wire were opposite to those of the paper, as illustrated by the dotted lines in figure 3(a). The developed process could minimize the accumulated strain on the paper for uniform winding of the silver-plated wire, which provided reliable performance of the battery. The lathe-based manufacturing process allowed for 300 mm-long batteries to be fabricated within 3 min. With minor modification, the process can be made roll-to-roll for producing an infinitely long battery.

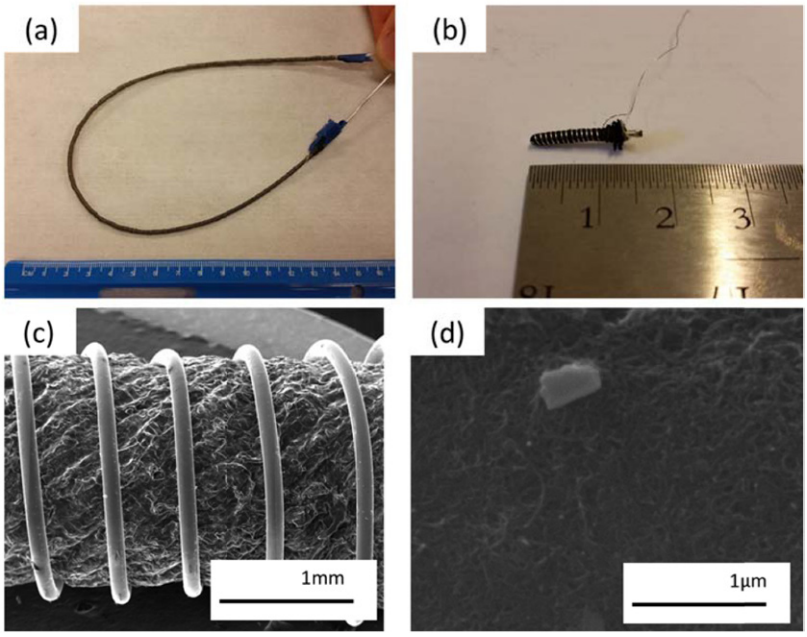

Figure 4. Cable-shaped batteries. (a) 300 mm-long battery, (b) 10 mm-long battery, (c) SEM image of a 10 mm-long battery and (d) MWCNT matrix of a 10 mm-long battery.

The batteries were activated by depositing electrolyte using a pipette or by immersion in electrolyte. Capillary flow allowed electrolyte to infiltrate the entire paper layers. In this study, the battery was activated by depositing electrolyte so that the consumed volume of electrolyte could be measured. For performance characterization according to various lengths, the batteries were cut using wire cutters to 300, 150, 80, 40, 20, and 10 mm. When the length was smaller than 10 mm, the battery performance was not stable because the wrapped copper wire started to unravel and became loose. Under various external loads, the voltage and current were measured with the multimeter for the various lengths of batteries. The external resistances were 0, 10, 100, 1000, 10 000 and ∞ Ω. For activation, 10 μl of phosphate-buffered saline (PBS) (1 $\times$ PBS; 7.4 pH; Life Technologies) was used for each 10 mm length of battery. For example, 300 μl of 1 $\times$ PBS was used for a 300 mm-long battery. The power per unit length was compared to evaluate the battery performance according to length.

To study the battery performance upon bending, a 20 mm-long battery was prepared. The battery was bent at the center of the longitudinal axis for 0, 45, 90, 135 and 170 degrees, and the voltage and current were measured with the multimeter under an external load of 384 Ω. For activation, 20 μl of 1 $\times$ PBS was used as the electrolyte.

To analyze the effect of electrolyte volume, a 10 mm-long battery was soaked with 0.5, 1, 2, 5, 10 and 25 μl of 1 $\times$ PBS. After depositing the electrolyte, enough time was given for the electrolyte to evaporate. Under an external load of 384 Ω, time-dependent voltage was measured with the multimeter. The results were presented in terms of generated energy for each volume. To measure electric power, 1 M-NaOH and 1 $\times$ PBS were tested, which were common reagents for biosensors. Human samples including blood, plasma, urine, saliva and whole blood were also tested as electrolytes. Urine and saliva were collected from de-identified volunteers. Plasma and blood samples with K2EDTA from de-identified donors were purchased from Bioreclamation. The multimeter was used to measure the voltage output from the batteries over time. The external load was 384 Ω. The measurement continued until the 10 μl solution drop completely evaporated and the voltage dropped to 0 V.

To demonstrate the generation of electric power, eight battery-cells were connected to operate an LED. The batteries were plugged into a breadboard and connected electrically using additional wires. Two sets of four battery cells in parallel connections were serially connected with 80 μl of 1 M-NaOH used as the electrolyte.

4. Results and discussion

Figures 4(a) and (b) show a 300 mm-long battery and a 10 mm-long battery, respectively. When the 300 mm-long cable-shaped battery was cut into smaller batteries, the individual batteries worked as a unit cell. When the battery was cut with wire cutters, the inner paper layer still worked as a separation layer, which did not cause short-circuiting to occur between the anode core and outside silver-plated copper wire. After cutting, a segment of the silver-plated copper wire could be unwrapped and used as the current collector for the cathode, while the unwrapped aluminum wire could be used as an anode terminal. Figures 4(c) and (d) show the images of a 10 mm-long battery and its magnified view by a scanning electron microscope (SEM). In the images, MWCNTs form a dense matrix under the silver-plated copper wire.

Figure 5(a) shows the voltage–current characteristic when the batteries of lengths 300, 150, 80, 40, 20, and 10 mm are subjected to loads of 0, 10, 100, 1000, 10 000 and ∞ Ω after addition of 1 $\times$ PBS. The open circuit voltage is 0.62–0.70 V, while the current in short-circuit is 15.2 mA for a 300 mm

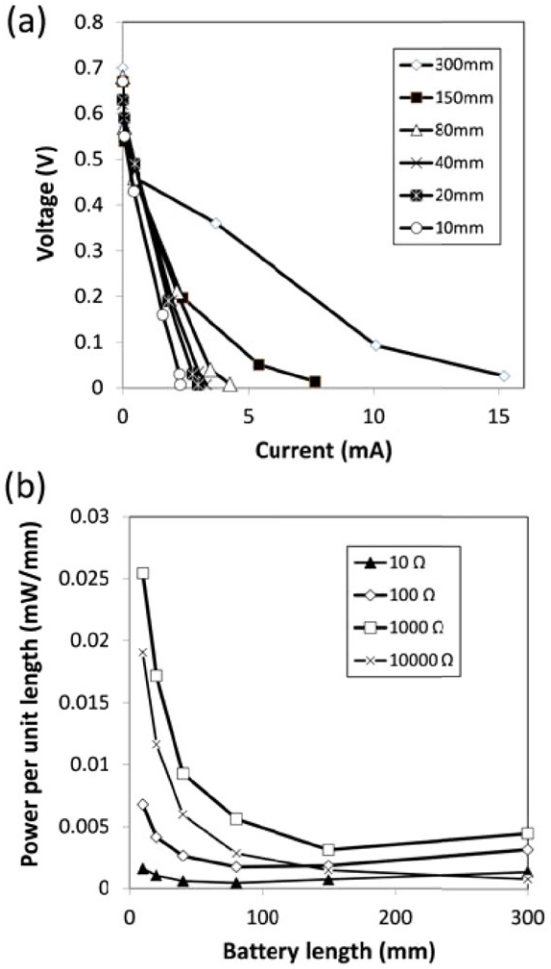

Figure 5. (a) Voltage–current characteristics for external loads of 0, 10, 100, 1000, 10 000 and ∞ Ω. The electrolyte of 1 × PBS (10 μl cm^{-1}) is applied for the batteries of 10–300 mm in lengths. (b) Power per unit length. At the external loads of 10, 100, 1000, and 10 000 Ω, the power per unit length decreases as the length of the batteries increases.

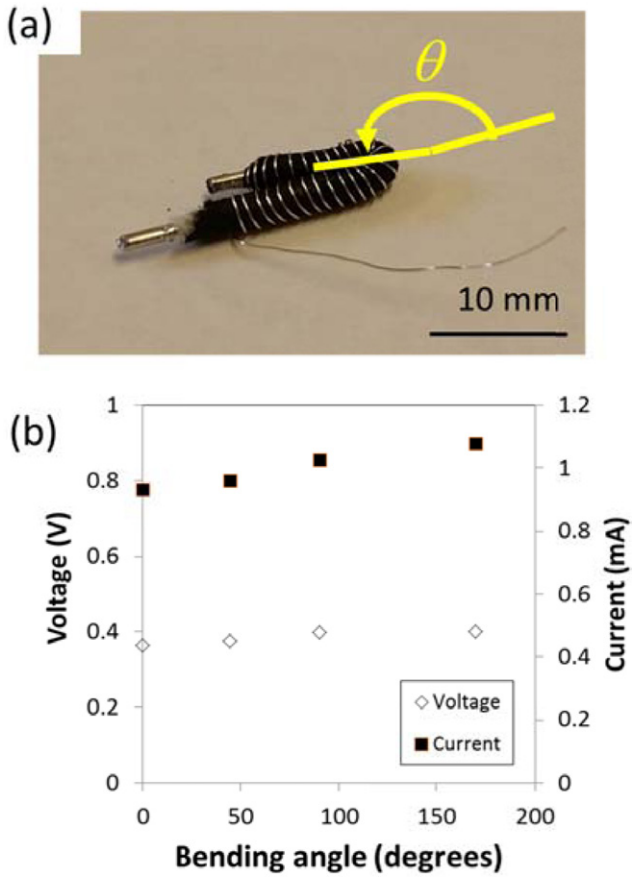

Figure 6. (a) 20 mm-long battery that is bent by 170°. The bending angle of θ is defined by the orientations of both ends of a battery. (b) Voltage and current according to bending for a 20 mm-long battery.

battery. As the length of the batteries is shortened, the current decreases due to the reduced surface area of the batteries. The maximum power is obtained for an external load of 100 Ω. For a 300 mm-battery, the maximum power is 1.33 mW at 100 Ω. The power per unit length is found to increase as the battery length decreases from 300 mm to 10 mm (figure 5(b)). The increased battery length could reduce the battery performance due to the increased resistance of the silver-plated copper wire. For a 300 mm-long battery, the measured resistance of the silver-plated copper wire was 2.0 Ω. The resistance of a silver-plated copper wire for a 10 mm-long battery was 0.07 Ω. Note that the resistance of the battery was dominated by the silver-plated copper wire rather than the aluminum wire. Resistance (R) is $\sigma l/A$, where σ is the resistivity, l is the length and A is the cross-sectional area. In comparison, the resistivity (σ) of the silver-plated copper wire was 1.6 times less than that of the aluminum wire. The length (l) of the silver-plated copper wire was 5.7 times greater than that of the aluminum wire. The cross-sectional area (A) of the silver-plated copper wire was 56 times less than that of the aluminum wire. As a result, the resistance of the silver-plated copper wire was 200 times greater than that of the aluminum wire in the battery.

A 20 mm-long battery was easily bent through the angles of 0, 45, 90, 135 and 170°. Figure 6(a) shows a battery bent by an angle of 170°. 20 μl of 1 × PBS was applied to a straight battery, and the voltage and current were measured for an external load of 384 Ω as the battery was bent progressively to 170°. As the bending angle increased, both voltage and current slightly increased by 9.5 and 15.7%, respectively (figure 6(b)). As the battery wire was bent, the silver-plated copper wire tightened and compressed the paper layers, reducing the thickness of the separation layer and increasing the electric current. In our SEM observation, the bent batteries showed a tight grip by the silver coated copper wire under bending (supporting information, table 1 in section S1 (stacks.iop.org/JMM/26/055011/mmedia)). At the bending angle of 160°, cellulose fibers were partially fractured due to the tension at the outside corner. Considering the low strength of the cellulose fibers, the tension upon bending induced the fracture of the fibers. Considering the disposable nature of the presented battery, the partial fracture may not be a problem without loss of battery power as observed in figure 6(b). To limit potential issues, the bending angle should be restricted to 90°.

To validate the voltage dependency on the wrapping tightness, the silver-plated copper wire was loosened for a

10 mm-long battery. The generated voltage was reduced by 67% because of the increase of the internal resistance and the larger diffusion length between the current collectors (supporting information; figure S1 in section S2 (stacks.iop.org/JMM/26/055011/mmedia)). To obtain more consistent performance, high tension should be applied when wrapping the silver-plated copper wire in manufacturing. Since the power is also dependent on electrolytes, a voltage regulator needs to be used when precise voltage is required.

For a 10 mm-long battery, various volumes of electrolyte, ranging from 0.5 to 25 μl were supplied sequentially to determine the effect on power production. Drops of various volumes of 1 M-NaOH were supplied to a battery. Using a load of 384 Ω, the voltage was measured for each drop until the drop completely evaporated. The next drop was then supplied. Figure 7(a) shows the time-dependent voltages for 0.5, 1, 2.5, 5, 10, 25 and 10 μl of the electrolyte. When a drop was supplied, the voltage rapidly increased and started to decrease as the drop evaporated. The peak voltage increased with an increase of volume up to 10 μl. When the volume increased to 25 μl, the area under the voltage curve increased. During evaporation, the voltage initially decreased with evaporation of the electrolyte but then increased temporally. This could possibly be caused by nonuniform evaporation in the paper layers. The maximum power was over 1.5 mW when the volume was over 10 μl.

Figure 7(b) shows the total energy that is produced for the volumes ranging from 0.5–25 μl. Four different batteries were used to measure the total energy. When the volume was under 10 μl, the total energy was smaller than 11 μWh because the bilayer was not fully soaked and the delivery of hydroxide ions to the anode was limited. When the volume was greater than 10 μl for a 10 mm-long battery, the papers appeared to be fully soaked and the generated energy increased with the increase of the supplied volumes. The produced energy was proportionally increased because a larger volume of NaOH could react with a larger amount of aluminum ions.

Figure 8(a) shows the time-dependent voltage generated by 10 μl aliquots of various electrolytes: blood, saliva, blood plasma, urine, 1 × PBS and NaOH. When blood and saliva were supplied for a 10 mm-battery with a load of 384 Ω, the load potential was smaller than 0.2 V. When blood plasma and urine were supplied, the load voltage increased to 0.3 V, which was similar to 1 × PBS. 1 M NaOH showed the highest voltage due to the abundance of hydroxide ions. Overall, the duration of power production for 10 μl drops ranged from 10 to 30 min. The variation in the voltages provided by the various electrolytes could be caused by varying ion concentrations within the solution drops. In addition, samples of saliva and blood showed the lowest power, possibly due to their high viscosity that might limit the transport of ions.

Using NaOH as electrolyte, an LED was powered by the parallel and serial connections of the batteries (figure 8(b)). A total of eight batteries were conveniently connected on a breadboard, with four connected in parallel and these two groups then connected in series. After addition of 10 μl of 1 M NaOH per battery, the LED light was powered for 10 min until the battery was completely dried (inset of figure 8(b)). Note that the LED light could also be powered by two batteries that

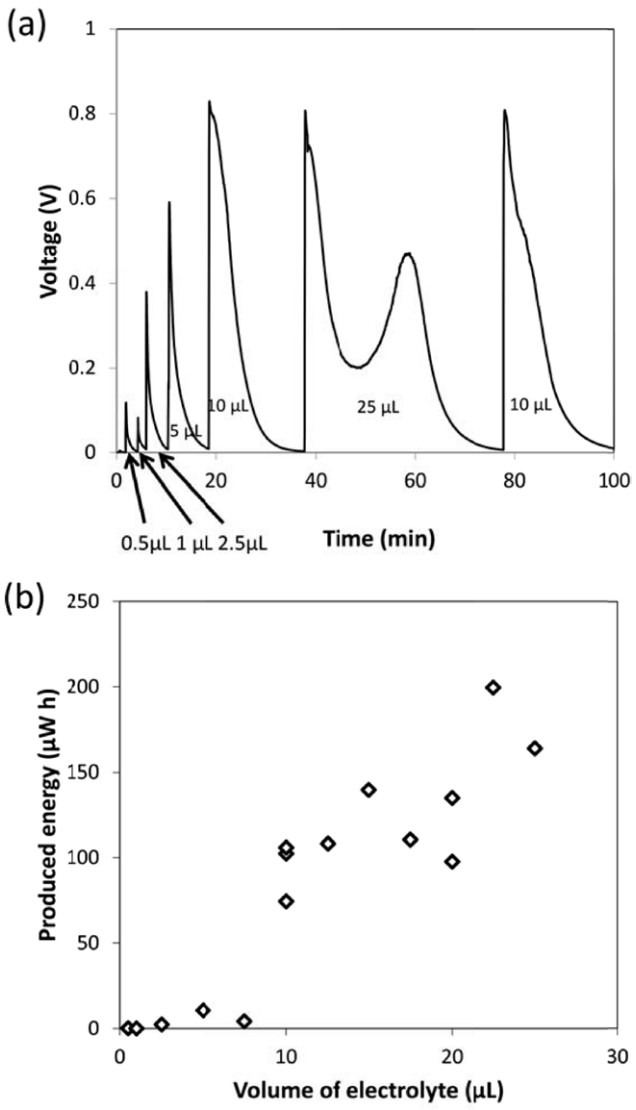

Figure 7. (a) Voltage change according to time due to input volumes of 1 × PBS (b) Generated energy for various volumes between 0.5 and 25 μl. The scatter plot is generated from four different batteries.

were serially connected (supporting information; figure S2 in section S3).

The role of MWCNTs in the battery is to catalyze the generation of hydroxide ions to increase the current. When batteries wrapped with the CNT-paper matrices of 50, 10 k and ∞ Ω/□ were tested, the electric current was significantly greater for the 50 Ω/□ battery (supporting information; figure S2 in section S4). Note that the sheet resistance of 50 Ω/□ was the smallest value that we could obtain in the MWCNT deposition. At this resistance, the cellulose paper was fully saturated with MWCNTs. Additional MWCNTs fell from the MWCNT-paper matrix during the wrapping process using a lathe. Considering that negligible power was produced from the battery without CNTs (∞ Ω/□), the catalytic performance of the silver-plated copper wire was clearly much lower than that of CNTs. With further optimization and functionalization of the CNTs, the electric power can be further improved [20].

The battery was activated by wetting the surface with water-based liquid samples. When over 10 μl of 1 M-NaOH

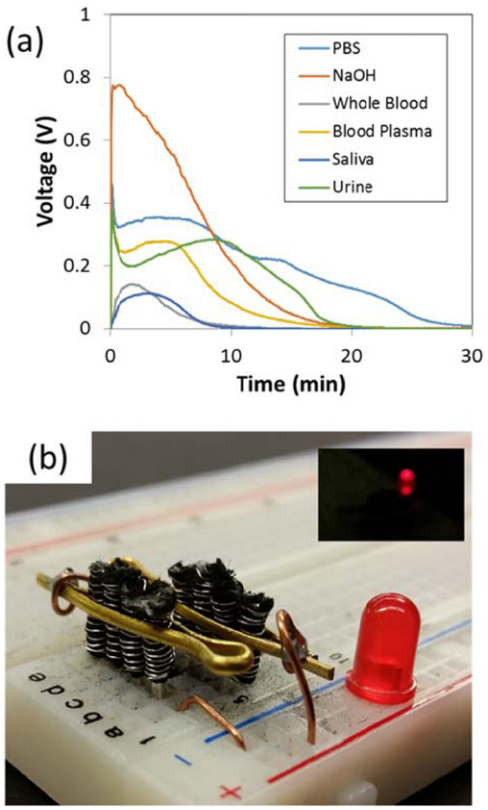

Figure 8. (a) Time-dependent voltage generation for various biological fluids and reagents; whole blood, saliva, urine, blood plasma, 1 × PBS and 1 M-NaOH. (b) Eight batteries connected to power an LED. Two sets of four batteries that are connected in parallel are connected in series. The inset shows the powered LED. Each battery is 10 mm in length.

was used, power was generated over 10 min until the liquid evaporated completely. When the battery was completely immersed in 1 × PBS or 1 M-NaOH, the power was continuously generated over 20 h but decreased with the generation of aluminum hydroxide. Such operation would be sufficient for portable POC devices (supporting information; section S5). The parasitic formation of hydrogen at the aluminum surface increased the corrosion of aluminum and the Ohmic resistance in the cell [21], which decreased the electric power. Considering power generation was due to the reaction of hydroxide ions with aluminum, the concentrations of PBS did not affect the voltage significantly. The open circuit voltage using 10 × PBS was higher than that using water by 0.1 V (supporting information; section S6). To enhance the lifetime and the power, aluminum alloys and nanostructures [22–24] can reduce the corrosion issues.

The characteristics of the cable-shaped battery presented here make it applicable to portable sensors and devices. Pacemakers [25], glucose sensors [26, 27] and simple electrical detection systems [28] require less than 1 mW [28], while gas sensors need less than 10 mW [29]. Our previous sensors developed for POC diagnostics detected targets by fluorescent measurement [30–32]. With the rapid development of low-cost optics, portable fluorescent microscopes can be powered by less than 5 mW [32]. Electrical detection is favored for POC devices due to their low power requirements [31]. Since the battery described here is disposable and inexpensive, it may be implemented into single-use devices. The battery is also activated by absorbing common reagents and biofluids, which enables simple and convenient operation of field-deployable devices. Considering potentially toxic and contagious nature of reagents and biosamples, the activation through absorption is more advantageous than placement of the liquid drop on a film-typed battery. The bendable shape and the plug-in configuration offer flexibility of the battery format for easy integration into devices.

Recently, a disposable battery was developed for biodevices [8], which was activated by consuming electrolytes or biofluids. The maximum energy and power densities were 1.07 μWh mm^{-3} and 83.4 μW mm^{-3}. The maximum energy density and the power density of a 10 mm-long battery were 4.3 μWh mm^{-3} and 73.4 μW mm^{-3}, respectively. Considering the total generated energy of 497 μWh in figure 7(a) and the consumed aluminum of 0.3 mg, the energy density based on consumed aluminum was 1.66 Wh g^{-1}, which was comparable to other Al–air systems that ranged from 1.34 to 1.99 Wh g^{-1} [33]. The equivalent energy density of the cable-shaped battery meant that the pristine MWCNTs worked effectively to catalyze the generation of hydroxide ions. In addition, the simple configuration of the battery allowed for easy extension to increase current and voltage using breadboard-type connections as demonstrated in figure 8. This versatile configuration can satisfy a wide variety of demands. Furthermore, the manufacturing can be performed without microfabrication facilities, which makes manufacturing inexpensive and scalable.

In our future work, new materials can be integrated into this manufacturing process to further improve the cable-shaped battery performance. Metals such as gold, silver, and platinum have shown catalytic potential for O_2 cathodes [34, 35]. The use of CNTs, manganese oxide nanostructures, or metal nanoparticles can increase oxygen reduction [36, 37]. Distributed on a paper matrix, these materials can improve the cable-shaped Al–air battery system.

5. Conclusion

A cable-shaped Al–air battery was fabricated to provide power to POC devices. A paper matrix embedded with MWCNTs was wrapped around an aluminum wire to catalyze the cathode reaction. To improve electrical conduction, a silver-plated copper wire was wrapped around the nanomaterial-Al wire. A simple, low cost manufacturing process using a lathe was developed to fabricate a 300 mm-long battery, which was reproducible and scalable. For electrical characterization, the battery was activated with PBS, NaOH, blood plasma, urine, saliva, and blood, which are frequently used with POC devices. The electric power of a 10 mm-battery was over 1.5 mW, which was enough to operate an LED by serial connection of two groups of four-10 mm cells in parallel. Considering the materials, performance, flexibility, and ease of manufacturing, the cable-shaped battery will facilitate convenient use of various formats of field-deployable POC devices.

References

[1] Chin C D, Linder V and Sia S K 2012 Commercialization of microfluidic point-of-care diagnostic devices *Lab Chip* **12** 2118–34

[2] Sia S K and Kricka L J 2008 Microfluidics and point-of-care testing *Lab Chip* **8** 1982–3

[3] Ge S, Ge L, Yan M, Song X, Yu J and Liu S 2013 A disposable immunosensor device for point-of-care test of tumor marker based on copper-mediated amplification *Biosens. Bioelectron.* **43** 425–31

[4] Bearinger J P, Dugan L C, Baker B R, Hall S B, Ebert K, Mioulet V, Madi M and King D P 2011 Development and initial results of a low cost, disposable, point-of-care testing device for pathogen detection *IEEE Trans. Biomed. Eng.* **58** 805–8

[5] Kong Y, Wang C Y, Yang Y, Too C O and Wallace G G 2012 A battery composed of a polypyrrole cathode and a magnesium alloy anode—toward a bioelectric battery *Synth. Met.* **162** 584–9

[6] Zloczewska A and Jonsson-Niedziolka M 2013 Efficient air-breathing biocathodes for zinc/oxygen batteries *J. Power Sources* **228** 104–11

[7] Stolarczyk K, Lyp D, Zelechowska K, Biernat J F, Rogalski J and Bilewicz R 2012 Arylated carbon nanotubes for biobatteries and biofuel cells *Electrochim. Acta* **79** 74–81

[8] Garay E F and Bashirullah R 2015 Biofluid activated microbattery for disposable microsystems *J. Microelectromech. Syst.* **24** 70–9

[9] Liu H and Crooks R M 2012 Paper-based electrochemical sensing platform with integral battery and electrochromic read-out *Anal. Chem.* **84** 2528–32

[10] Baptista A C, Martins J I, Fortunato E, Martins R, Borges J P and Ferreira I 2011 Thin and flexible bio-batteries made of electrospun cellulose-based membranes *Biosens. Bioelectron.* **26** 2742–5

[11] Mano N, Mao F and Heller A 2003 Characteristics of a miniature compartment-less glucose-O-2 biofuel cell and its operation in a living plant *J. Am. Chem. Soc.* **125** 6588–94

[12] Sakai H, Nakagawa T, Tokita Y, Hatazawa T, Ikeda T, Tsujimura S and Kano K 2009 A high-power glucose/oxygen biofuel cell operating under quiescent conditions *Energy Environ. Sci.* **2** 133–8

[13] Jimbo H and Miki N 2008 Gastric-fluid-utilizing micro battery for micro medical devices *Sensors Actuators* B **134** 219–24

[14] Pushparaj V L, Shaijumon M M, Kumar A, Murugesan S, Ci L, Vajtai R, Linhardt R J, Nalamasu O and Ajayan P M 2007 Flexible energy storage devices based on nanocomposite paper *Proc. Natl Acad. Sci. USA* **104** 13574–7

[15] Lee K B 2006 Two-step activation of paper batteries for high power generation: design and fabrication of biofluid-and water-activated paper batteries *J. Micromech. Microeng.* **16** 2312

[16] Lee K B 2005 Urine-activated paper batteries for biosystems *J. Micromech. Microeng.* **15** S210–4

[17] Kwon Y H *et al* 2012 Cable-type flexible lithium ion battery based on hollow multi-helix electrodes *Adv. Mater.* **24** 5192–7

[18] Zou D C, Wang D, Chu Z Z, Lv Z B and Fan X 2010 Fiber-shaped flexible solar cells *Coord. Chem. Rev.* **254** 1169–78

[19] Park J, Park M, Nam G, Lee J S and Cho J 2015 All-solid-state cable-type flexible zinc-air battery *Adv. Mater.* **27** 1396–401

[20] Cheng F Y and Chen J 2012 Metal–air batteries: from oxygen reduction electrochemistry to cathode catalysts *Chem. Soc. Rev.* **41** 2172–92

[21] Wang H Z, Leung D Y C, Leung M K H and Ni M 2010 Modeling of parasitic hydrogen evolution effects in an aluminum–air Cell *Energy Fuels* **24** 3748–53

[22] Smoljko I, Gudic S, Kuzmanic N and Kliskic M 2012 Electrochemical properties of aluminium anodes for Al/air batteries with aqueous sodium chloride electrolyte *J. Appl. Electrochem.* **42** 969–77

[23] Tang Y G, Lu L B, Roesky H W, Wang L W and Huang B Y 2004 The effect of zinc on the aluminum anode of the aluminum–air battery *J. Power Sources* **138** 313–8

[24] Li C S, Ji W Q, Chen J and Tao Z L 2007 Metallic aluminum nanorods: synthesis via vapor-deposition and applications in al/air batteries *Chem. Mater.* **19** 5812–4

[25] Lueke J and Moussa W A 2011 MEMS-based power generation techniques for implantable biosensing applications *Sensors* **11** 1433–60

[26] Croce R A *et al* 2013 A miniaturized transcutaneous system for continuous glucose monitoring *Biomed. Microdevices* **15** 151–60

[27] Liao Y T, Yao H F, Lingley A, Parviz B and Otis B P 2012 A 3 μW CMOS glucose sensor for wireless contact-lens tear glucose monitoring *IEEE J. Solid-State Circuits* **47** 335–44

[28] Zhang M, Haider M R, Huque M A, Adeeb M A, Rahman S and Islam S K 2007 A low power sensor signal processing circuit for implantable biosensor applications *Smart Mater. Struct.* **16** 525–30

[29] Cook K A, Albano F, Nevius P E and Sastry A M 2006 POWER (power optimization for wireless energy requirements): a MATLAB based algorithm for design of hybrid energy systems *J. Power Sources* **159** 758–80

[30] Kim J-H *et al* 2012 Immunosensor towards low-cost, rapid diagnosis of tuberculosis *Lab Chip* **12** 1437–40

[31] Kim J-H, Hiraiwa M, Lee H-B, Lee K-H, Cangelosi G A and Chung J-H 2013 Electrolyte-free amperometric immunosensor using a dendritic nanotip *RSC Adv.* **3** 4281–7

[32] Inoue S *et al* 2014 Semi-automated, occupationally safe immunofluorescence microtip sensor for rapid detection of mycobacterium cells in sputum *Plos One* **9** e86018

[33] Revel R, Audichon T and Gonzalez S 2014 Non-aqueous aluminium-air battery based on ionic liquid electrolyte *J. Power Sources* **272** 415–21

[34] Wu G, More K L, Johnston C M and Zelenay P 2011 High-performance electrocatalysts for oxygen reduction derived from polyaniline, iron, and cobalt *Science* **332** 443–7

[35] Wang T, Kaempgen M, Nopphawan P, Wee G, Mhaisalkar S and Srinivasan M 2010 Silver nanoparticle-decorated carbon nanotubes as bifunctional gas-diffusion electrodes for zinc-air batteries *J. Power Sources* **195** 4350–5

[36] Gupta N, Toh T, Fatt M W, Mhaisalkar S and Srinivasan M 2012 Paper like free-standing hybrid single-walled carbon nanotubes air electrodes for zinc-air batteries *J. Solid State Electrchem.* **16** 1585–93

[37] Cheng F Y, Shen J, Ji W Q, Tao Z L and Chen J 2009 Selective synthesis of manganese oxide nanostructures for electrocatalytic oxygen reduction *ACS Appl. Mater. Interfaces* **1** 460–6